J. Phys. B: At. Mol. Opt. Phys. **40** (2007) 2563–2576 doi:10.1088/0953-4075/40/13/003

Coplanar symmetric and asymmetric electron impact ionization studies from the $1b_1$ state of H_2O at low to intermediate impact energies

Christian Kaiser[1], Dustin Spieker[2], Junfang Gao[2], Martyn Hussey[1], Andrew Murray[1] and Don H Madison[2]

[1] School of Physics and Astronomy, University of Manchester, Manchester M13 9PL, UK
[2] Department of Physics, University of Missouri-Rolla, Rolla, MO 65409, USA

Received 29 March 2007, in final form 30 March 2007
Published 15 June 2007
Online at stacks.iop.org/JPhysB/40/2563

Abstract

(e, 2e) ionization differential cross sections are presented for incident electron energies ranging from 15 eV to 95 eV above the ionization threshold of the $1b_1$ molecular state of H_2O. Experimental results and theoretical analysis were derived for three energies in a coplanar symmetric geometry, and for three energies in an asymmetric geometry. The experimental data show a wide variation in the cross section over this range of energies, whereas the theoretical analysis carried out using a sophisticated molecular DWBA model, which includes the final state post collision interaction (PCI), shows best agreement at lower energies. The experimental techniques used to collect the data are described here as well as an improved theoretical approach using elastic scattering cross sections to evaluate the accuracy of the distorted waves utilized in the calculation of the ionization cross sections.

1. Introduction

Ionization of atomic and molecular targets is one of the most complex and fundamental collision processes that can be studied in detail. These ionizing collisions are important in a wide range of different areas, ranging from plasma physics, astrophysics, atmospheric physics, medical and biological processes involving low energy electrons, to the study of high voltage discharges. To fully characterize these interactions, it is necessary to perform sophisticated measurements where an incident electron of well-controlled momentum scatters and ionizes the target. The scattered electron is then detected in time-correlated coincidence with either the electron ejected during ionization, or with the resulting ion [1–5].

In these (e, 2e) experiments, information about the collision process is obtained by measuring the outgoing momenta of the collision products. This is usually accomplished by determining a cross section that is five-fold differential in angle and energy. In some cases, the spins of the ingoing and outgoing electrons are measured, and so information about spin

exchange and spin flip processes can be ascertained, however in most experiments presently conducted the spin of the electrons is not measured.

For molecular targets, it is very difficult to know the orientation and alignment of the molecule prior to the interaction occurring, unless this can be defined prior to the collision or can be measured following the collision. In most cases, this means that an averaging over the orientation of the target must be included in calculations that compare with experimental results. Hence there is loss of information about the collision process for these systems. Most theoretical calculations adopt approximations when calculating the averaged cross sections for these targets [6–9], which again can lead to uncertainty when comparing theory to experiment.

At high incident electron energies, there has been a large body of data accumulated on the ionization of molecular targets using electron momentum spectroscopy (EMS), as pioneered by Weigold and McCarthy [1, 10, 11]. These experiments adopt a high incident beam energy so that impulse and distorted wave calculations of the reaction process can be carried out to high accuracy, so as to determine the momentum profile of the bound electron ejected during ionization. In this way, different models of the molecular bound state wavefunction can be tested, and a description of the molecular geometry generated. Such experiments have been successfully employed for both simple and complex molecular systems, and this technique continues to be a powerful method used to determine molecular structure.

By contrast, the interaction of low to intermediate energy electrons with molecular targets has been much less studied. This energy region (from threshold to ∼200 eV) is important as it is here that the cross section for ionization is largest. Approximations which are accurate at high impact energies can no longer be applied, and so there are stringent demands on theory which must be satisfied for accurate comparison with experimental data.

Most experiments carried out in this energy region have studied atomic targets, as there is much that can be learned about the ionization process using these simpler systems. Atomic targets can be described using a spherical basis centred on the nucleus, and so it is possible to apply a partial wave analysis to describe the ingoing and outgoing electrons involved in the interaction. By contrast, molecular systems have spatially distributed nuclei, making theoretical analysis and computational models of the interaction far more demanding.

Experiments on molecular targets often employ effusive beams produced at room temperature, and so these targets may have internal rotational and vibrational energy. The ionization potential from these ground ro-vibrational states is usually less defined than for atomic targets, due to the associated Franck–Condon overlap between the potential energy curves of the neutral molecules and the resulting ions. The (e, 2e) coincidence signal for molecules may then have a correspondingly lower yield compared to an atomic target where the ionization potential is well defined.

Although a full description of the ionization process for molecular systems at these energies is not possible at present, much can still be learned within these limitations. New experiments are being conducted using different molecular targets, whereas new and sophisticated theories are under development to allow comparisons to be made between theory and experiment. Measurements have been made using diatomic targets including H_2 and N_2 [12–18], and for polyatomic targets including CO_2 and H_2O [19, 20]. In this paper, further results are presented for an H_2O target at significantly lower energies than has been studied before. A coplanar geometry was chosen for these studies, and results are presented for both coplanar symmetric and coplanar asymmetric geometries, with incident energies ranging from 15 eV to 95 eV above the ionization threshold of the $1b_1$ state of neutral H_2O. This state was chosen as it is well resolved in energy, and has been studied by previous workers in this area for comparison.

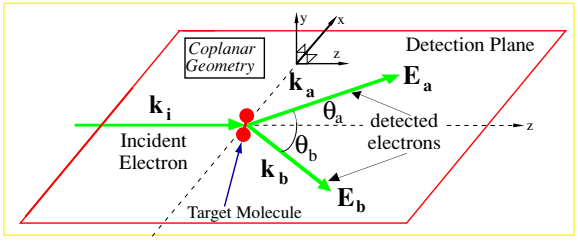

Figure 1. The coplanar geometry chosen for the studies detailed here. (θ_a, θ_b) are the angles of the electron analysers with respect to the incident beam direction $\mathbf{k}_0$. For coplanar symmetric geometries, $\theta_a = \theta_b$. For asymmetric geometries, θ_a is fixed at $\theta_a = 22^\circ$ while analyser 2 is swept around the scattering plane.

(This figure is in colour only in the electronic version)

The paper is divided into five sections. Following this introduction, the experimental setup is described, including the techniques adopted to produce a molecular beam of H_2O that was uncontaminated by background gas. The theoretical analysis which is adopted is then described, and methods used to include correlation, polarization and exchange distortion of the molecule are discussed. The results from experiment and theory are detailed, and comparisons made. A summary of this work is then given, and conclusions drawn as to future studies which are required.

2. Experimental setup

The experiments which are described here were carried out in the fully computer controlled and computer optimized (e, 2e) spectrometer that operates in Manchester. This apparatus has been described in detail elsewhere [21–24], and has been designed to operate in the energy regime from ∼10 eV to ∼300 eV. The spectrometer allows measurements to be conducted from a coplanar geometry through to the perpendicular plane [21], although in the present measurements only the coplanar geometry was used. The power supplies for the electrostatic lenses that control the electron gun and electron detectors are fully computer controlled, and so the spectrometer can be operated for 24 h/day without the need for operator intervention.

For the coplanar symmetric experiments described here, the electron detectors were moved so that their angles (θ_a, θ_b) with respect to the incident beam direction were equal to each other throughout the measurements (see figure 1). In this configuration, the energies selected for the scattered and ejected electrons were equal. The incident electron energy was set to 20 eV, 40 eV and 60 eV above the ionization potential from the $1b_1$ state, which is around 12.6 eV. The angles that could be accessed in this configuration ranged from $\theta_a = \theta_b = 25^\circ$ through to $\theta_a = \theta_b = 135^\circ$.

For coplanar asymmetric experiments, analyser 1 was fixed at a scattering angle $\theta_a = 22^\circ$, while analyser 2 was swept around the scattering plane. In this case, analyser 2 detected electrons with fixed energy of 5 eV, whereas analyser 1 detected electrons with energies of 10 eV, 50 eV and 90 eV so as to cover a range of energies from low to intermediate energies. The fixed scattering angle $\theta_a = 22^\circ$ was chosen as this was the smallest angle that could be used without the incident electron beam from the gun striking the side of the analyser (and so producing unacceptable levels of noise on the coincidence signal). The range of angles which could be accessed in this configuration ranged from $\theta_b = 30^\circ$ to 140° (forward scattering) and from $\theta_b = 225^\circ$ to 290° (the backscattering direction).

The energy resolution of the spectrometer is set by the resolution of the electron gun and the pass energy of the analysers. The electron gun used two electro-static lenses to deliver a quasi-collimated beam with an energy resolution ∼0.5 eV, a beam angle of 0° and a pencil angle of 2°. The analyser pass energy was then set to measure electrons so that the overall resolution of the coincidence signal (as measured using a helium atomic target) was 600 meV. The acceptance angle of the analyser lenses was ±3°, as set by input apertures at the entrance to the electrostatic lenses.

Production of a high quality molecular beam of H_2O required careful monitoring of the experiment as it progressed. Pure liquid water was initially loaded into a spherical glass flask which was connected to a 12 l s^{-1} roughing pump. The pump removed background gas from the flask, and extracted dissolved gases held in the water. This de-gassing procedure was carried out for ∼2 h before the water sample was used in the experiment, to ensure that the proportion of dissolved gases in the water was minimized. A glass flask was used for this procedure as this allowed the process to be visually monitored.

The de-gassed water was then transferred to a 150 mm long tubular stainless steel flask which was connected to the main vacuum system using a swagelok fitting. The inner diameter of this flask was 9 mm, and the outside diameter was 12.7 mm, so that a standard swaged fitting could be used. The flask was secured to the 'cold' side of a 50 mm × 50 mm thermo-electric cooler (TEC) using a large aluminium block, and the assembly (flask + block) was insulated from the air using Styrofoam. The 'hot' side of the TEC was attached using thermal conducting paste to an aluminium heatsink to which a 12VDC boxer fan was secured, so that heat from the TEC could be dissipated efficiently.

An AD590 sensor was secured to the aluminium block surrounding the flask, so that the temperature of the insulated assembly could be monitored and controlled. This was accomplished using a Newport model 325 temperature controller [25], which supplied drive current to the TEC. The controller held the temperature of the water at a constant value of 23 °C ± 0.1 °C throughout data collection.

To monitor the molecular beam inside the vacuum chamber which was produced from the water, a quadrupole mass spectrometer was installed onto the spectrometer. This proved invaluable, as it was then possible to continuously monitor the background gases in the chamber during operation. All experiments were performed with a ratio of H_2O to N_2 (and other gases) of >30:1. If this ratio reduced, the experiment was halted and the water changed to a newly de-gassed sample. Typical partial pressures in the vacuum chamber during operation were $H_2O = 5.2 \times 10^{-6}$ Torr, $N_2 = 6 \times 10^{-8}$ Torr, $O_2 = 4.9 \times 10^{-8}$ Torr.

Figure 2 shows a typical coincidence energy spectrum obtained from the experiment during operation. In this example, the analysers were set to pass electrons of energy 20 eV, and a symmetric geometry was chosen with $\theta_a = \theta_b = 45°$. The $1b_1$, $3a_1$ and $1b_2$ states are clearly resolved in this spectrum, which is fitted to three Gaussian peaks to ascertain the widths of the spectral profiles. In this case, the $1b_1$ state was found to have a width of 620 meV, which is comparable to that for an atomic target. This indicates that the energetic effects of ro-vibrational transitions from the ground state to the ion state are negligible for this state. There is an offset of 1 eV in the position of the peaks which is due to contact potentials in the spectrometer.

The experiments were carried out over a period of 5 months, using electron beam currents ∼200 nA for all data runs. Over this period of time, the filament current driving the cathode had to be steadily decreased, as the water vapour within the vacuum chamber slowly reduced the diameter of the filament. At commencement of experimentation, the filament current was 2100 mA for a delivered beam current of 200 nA, whereas after 5 months the operating current of the filament had reduced to 1020 mA for the same beam current. These changes occurred

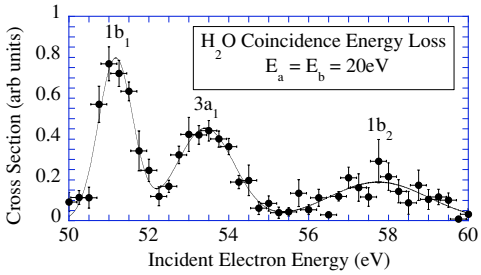

Figure 2. Coincidence energy loss spectrum from H_2O for a coplanar symmetric geometry and an outgoing electron energy of 20 eV for each electron. The data are fitted to three Gaussians, the $1b_1$ peak being chosen for study.

sufficiently slowly to allow regular adjustment. Further checks were made daily on the energy of the incident electron beam by monitoring the coincidence energy spectrum (figure 2), and regular monitoring of the partial pressures of the gases in the vacuum chamber was also carried out.

Figure 3 shows the results of experiments using a symmetric geometry. The data are normalized to unity at $\theta_a = \theta_b = \theta = 45^\circ$, since the results have not been placed on an absolute scale. Figure 3(a) shows the data at an excess energy 20 eV above the ionization threshold. In this case, there is a clear forward scattering lobe which appears to be composed of a double structure, with peaks at $\theta \sim 32.5^\circ$ and at $\theta \sim 45^\circ$. The minimum in the cross section occurs at $\theta \sim 80^\circ$, and a backscattering peak is seen which peaks at $\theta \sim 140^\circ$. The forward structure is larger than the backward peak by a ratio of $\sim 1.3 : 1$.

As the incident energy increases, the ratio of forward to backward scattering cross section increases, as has been seen for most atomic targets in this geometry. A two peak structure in the forward lobe is clearly seen for 60 eV excess energy (figure 3(c)), and is also visible at 40 eV excess energy (figure 3(b)), although the statistical variation in the data is significant at this energy. The variation in the forward lobe cross section compared to the peak in the backward direction is $\sim 2.8 : 1$ at 40 eV excess energy and is $\sim 3.2 : 1$ at 60 eV excess energy. The contrast between the maximum and minimum in the cross section increases as the energy increases. For 20 eV excess energy, this ratio is $\sim 4.1 : 1$, whereas at 40 eV and 60 eV excess energies this rises to $\sim 13 : 1$ and $\sim 32 : 1$, respectively.

The measured coplanar asymmetric data are shown in figure 4, again normalized to unity at $\theta_b = 45^\circ$. In this case the data are presented over the angular range from $\theta_b = 30^\circ$ to 290°, the region between $\theta_b = 140^\circ$ and $\theta_b = 225^\circ$ being inaccessible due to the position of the electron gun. Figure 4(a) shows the lowest energy results, with an incident energy 15 eV above the ionization threshold. A single forward lobe is seen which peaks at $\theta_b \sim 100^\circ$. A second peak occurs in the backscatter region, however the maximum of this peak appears to occur at $\theta_b < 225^\circ$.

As the incident energy is increased to 55 eV above threshold, the forward lobe splits into two clear peaks of approximately equal magnitude, as seen in figure 4(b). The peaks occur at $\theta_b \sim 40^\circ$ and 110°, whereas the minimum between these peaks is at $\theta_b \sim 70^\circ$. The measured cross section in the backscatter region now peaks at $\theta_b \sim 280^\circ$. As the energy increases further to 95 eV above threshold (figure 4(c)), the double peak in the forward direction is still visible but the magnitudes of the peaks are now different. The largest peak remains at $\theta_b \sim 40^\circ$, the second peak is once more at $\theta_b \sim 110^\circ$ however the minimum moves to $\theta_b \sim 85^\circ$. The results in the backward direction also have structure, with a minimum occurring when $\theta_b \sim 250^\circ$.

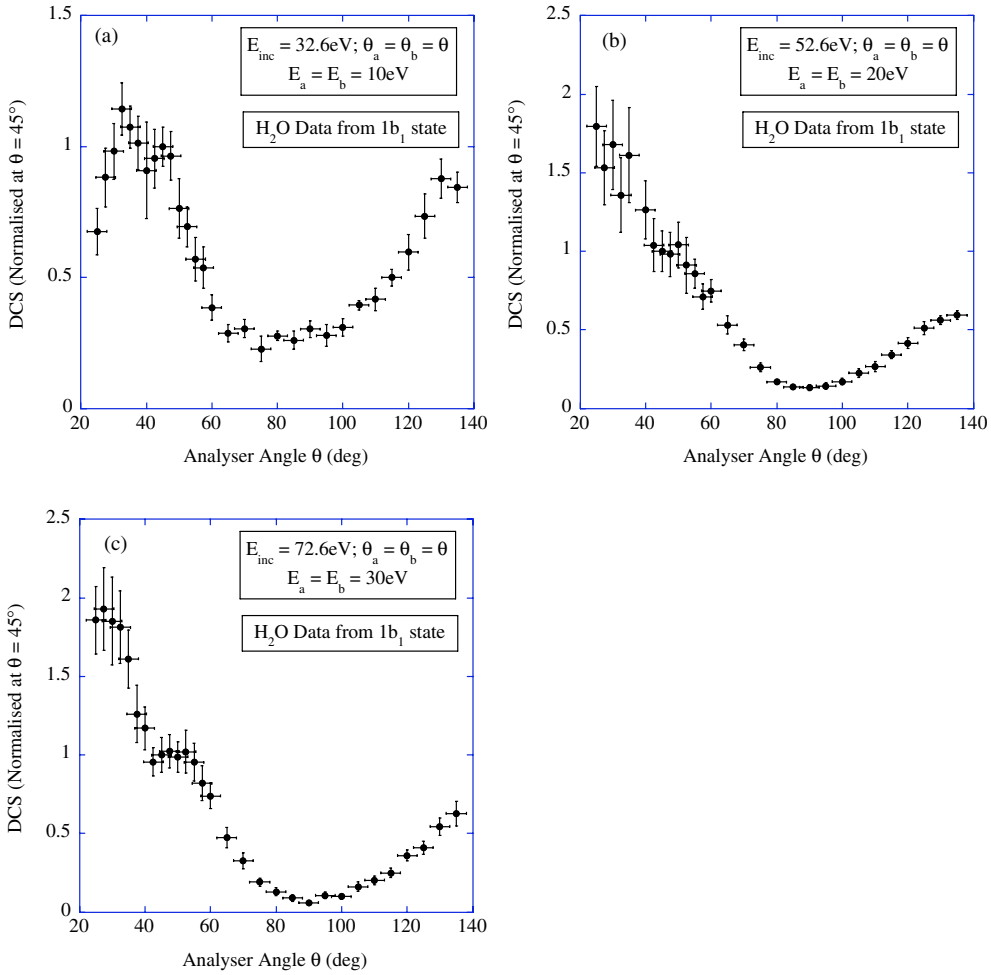

Figure 3. Experimental data using a coplanar symmetric geometry, at excess electron energies of 20 eV, 40 eV and 60 eV above the $1b_1$ ionization threshold. For details, see text.

3. Theory

The molecular three-body distorted wave (M3DW) approximation has been presented elsewhere [7, 26, 27] so only a brief overview will be presented here. The M3DW FDCS (fully differential cross section) is given by

$$\frac{\mathrm{d}^5\sigma}{\mathrm{d}\Omega_a\,\mathrm{d}\Omega_b\,\mathrm{d}E_b} = \frac{1}{(2\pi)^5}\frac{k_a k_b}{k_i}(|T_{\mathrm{dir}}|^2 + |T_{\mathrm{exc}}|^2 + |T_{\mathrm{dir}} - T_{\mathrm{exc}}|^2), \tag{1}$$

where $\vec{k}_i$ is the initial-state wave vector, $\vec{k}_a$ ($\vec{k}_b$) is the wave vector for the scattered (ejected) electron, and the direct and exchange amplitudes are T_{dir} and T_{exc}, respectively:

$$T_{\mathrm{dir}} = \left\langle \chi_a^-(\vec{k}_a, \mathbf{r}_1)\chi_b^-(\vec{k}_b, \mathbf{r}_2)C_{\mathrm{scat-eject}}(r_{12})|V - U_i|\phi_j^{OA}(\mathbf{r}_2)\chi_i^+(\vec{k}_i, \mathbf{r}_1)\right\rangle \tag{2}$$

$$T_{\mathrm{exc}} = \left\langle \chi_a^-(\vec{k}_a, \mathbf{r}_2)\chi_b^-(\vec{k}_b, \mathbf{r}_1)C_{\mathrm{scat-eject}}(r_{12})|V - U_i|\phi_j^{OA}(\mathbf{r}_2)\chi_i^+(\vec{k}_i, \mathbf{r}_1)\right\rangle. \tag{3}$$

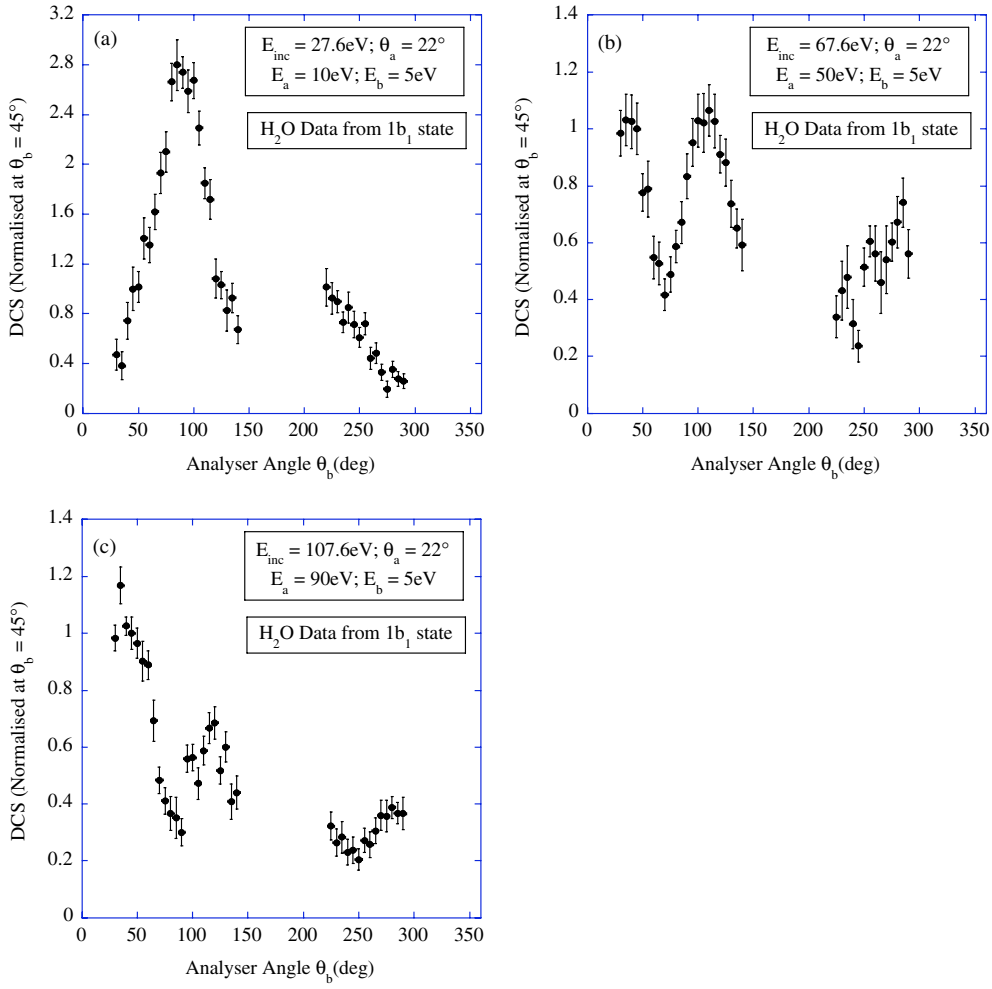

Figure 4. Experimental data using a coplanar asymmetric geometry, at excess electron energies of 15 eV, 55 eV and 95 eV above the $1b_1$ ionization threshold. For details, see text.

In equations (2) and (3), $\mathbf{r}_1$ ($\mathbf{r}_2$) is the co-ordinates of the incident (bound) electron, χ_i, χ_a, and χ_b are the distorted waves for the incident, scattered and ejected electrons respectively, ϕ_j^{OA} is the orientation-averaged molecular orbital (OAMO) [7] for the initial bound state of the molecule generated from molecular orbitals calculated using GAMESS [28], V is the initial-state interaction between the projectile and the neutral molecule, and U_i is the initial-state spherically symmetric distorting potential which is used to calculate the initial-state distorted wave χ_i. The $C_{\mathrm{scat-eject}}$ term is the Coulomb interaction between the scattered projectile and ejected electron. Since this post-collision interaction (PCI) term is included in the final state wavefunction, the effects of PCI are included to all orders of perturbation theory.

The initial-state molecular distorted waves are calculated using a spherically symmetric distorting potential U_i. The Schrödinger equation for the incoming electron wavefunction is given by

$$\left(T + U_i - \frac{k_i^2}{2}\right)\chi_i^+(\vec{k}_i, r) = 0, \tag{4}$$

where T is the kinetic energy operator, and the '+' superscript on $\chi_i^+(\vec{k}_i,\ r)$ indicates outgoing wave boundary conditions. The initial-state distorting potential contains three components $U_i = U_S + U_E + U_P$, where U_S is the initial-state spherically symmetric static potential which is obtained from the molecular charge density averaged over all angular orientations, U_E is the exchange-distortion potential, and U_P is the polarization potential.

For electron–molecule collisions, there are two different types of electron exchange that need to be considered. The first is exchange between the two continuum electrons and this is treated by the exchange amplitude $T_{\rm exc}$. The second exchange effect is exchange between the continuum electrons and the spectator bound state electrons which is treated through the exchange-distortion (ED) potential U_E. For the ED potential, we use the Furness–McCarthy [29] approximation which has been widely used for atomic scattering. In this approximation, the ED potential U_E depends on the molecular charge density

$$U_E = -\tfrac{1}{2}\left\{\left(k_i^2 - U_S\right) - \sqrt{\left(k_i^2 - U_S\right)^2 + 2\rho_S(r)}\right\}. \tag{5}$$

Here $\rho_S(r)$ is the spherically averaged molecular electronic charge density. The radial charge density is defined such that the integral over r yields the number of electrons in the molecule.

For the polarization potential U_P, we have used the correlation-polarization potential of Perdew and Zunger [30] (see also Padial and Norcross [31]). The two final channel distorted waves are obtained from a Schrödinger equation similar to equation (4)

$$\left(T + U_f - \frac{k_{a(b)}^2}{2}\right)\chi_{a(b)}^-(\vec{k}_{a(b)}, r) = 0. \tag{6}$$

Here $U_f = U_I + U_E + U_P$ where U_I is the final state spherically symmetric static distorting potential for the molecular ion which is calculated using the same procedure as U_S except that the active electron is removed from the charge distribution.

Since the distorted waves are obviously a critical component of the theoretical approach, it would be good to be able to evaluate their quality. One way to assess the quality of distorted waves is to look at elastic scattering cross sections. The distorted waves are obtained by summing a partial wave expansion to convergence and the partial wave phase shifts can be used to calculate elastic scattering cross sections. Figure 5 compares the resulting theoretical cross sections with absolute experimental data. In the figure, the dotted curve corresponds to using the static potential U_S only in the calculation of the distorted waves, the dashed curve corresponds to $U_S + U_P$ and the full curve corresponds to $U_S + U_P + U_E$. It is seen that polarization is more important than ED particularly for the lower energies. For the lowest energy, polarization increased the elastic scattering cross section by two orders of magnitude and ED increased the cross section by another factor of 2–3 to bring the magnitude of the theoretical results into qualitative agreement with experiment. Although the effects of polarization and ED decrease with increasing electron energy as one would expect, even for the higher energies, it is important to include at least polarization to get the proper magnitude for the elastic cross section.

The theoretical elastic scattering cross sections predict two minima for all energies that are not seen in the data. Previously we have used a phenomenological approximation for the polarization potential of the form

$$U_P^a = -\frac{\alpha_0}{2r^4}\left\{1 - \exp\left[-\left(\frac{r}{a}\right)^6\right]\right\}, \tag{7}$$

where α_0 is the dipole polarizability, and a is an adjustable parameter that acts as a cutoff radius for the polarization potential. We decided to see how well this potential would work for elastic scattering. In figure 6, the chain curves are elastic scattering cross sections obtained using

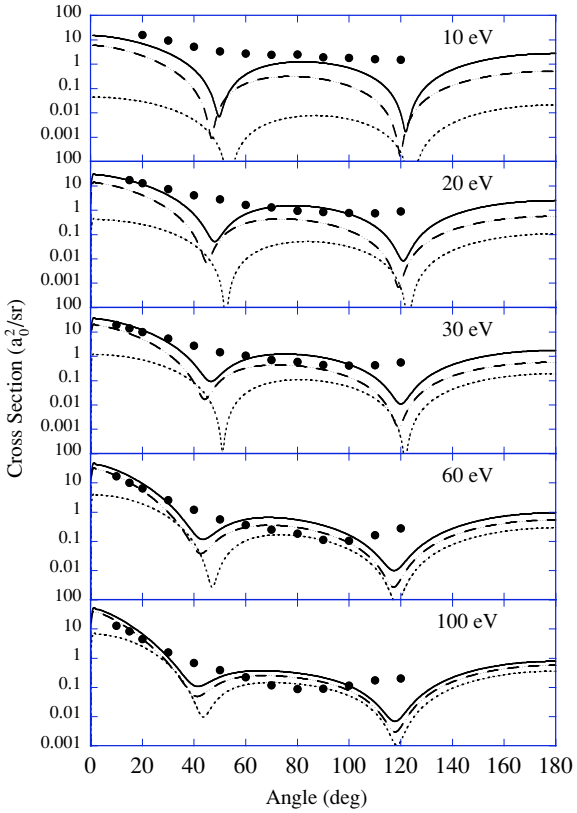

Figure 5. Elastic differential cross sections for electrons scattering from H_2O. The energy of the incident electron is noted in each panel. The experimental data are those of Danjo and Nishimura [32]. The theoretical curves are dotted, U_S; dashed, $U_S + U_P$; and solid, $U_S + U_P + U_E$.

equation (7) with the cutoff parameter (a) varied to give the best visual fit to the experimental data. As can be seen from the figure, this procedure yields cross sections in very good agreement with experiment for the lowest energy. Interestingly, instead of getting better with increasing energy as one would normally expect, the agreement gets worse with increasing energy. Nevertheless, adjustable parameter cross sections do not have the two minima that is predicted by the Perdew–Zunger correlation-polarization potential. Figure 7 presents a plot of the cutoff parameters which were used to calculate the cross sections shown in figure 6. As can be seen, the cutoff parameters decrease with increasing energy and range between 0.6 and 0.3 a_0 for this energy range which is smaller than we would have intuitively expected. They are also about four times smaller than the values used by Gao *et al* [6] for electron impact ionization of N_2.

4. Comparison between experimental data and theory

Figure 8 compares the theoretical and experimental results for the coplanar symmetric geometry. Since the experimental data are not absolute, both the data and theory are normalized to unity at the lowest angle peak. The dashed curve on the figures are results

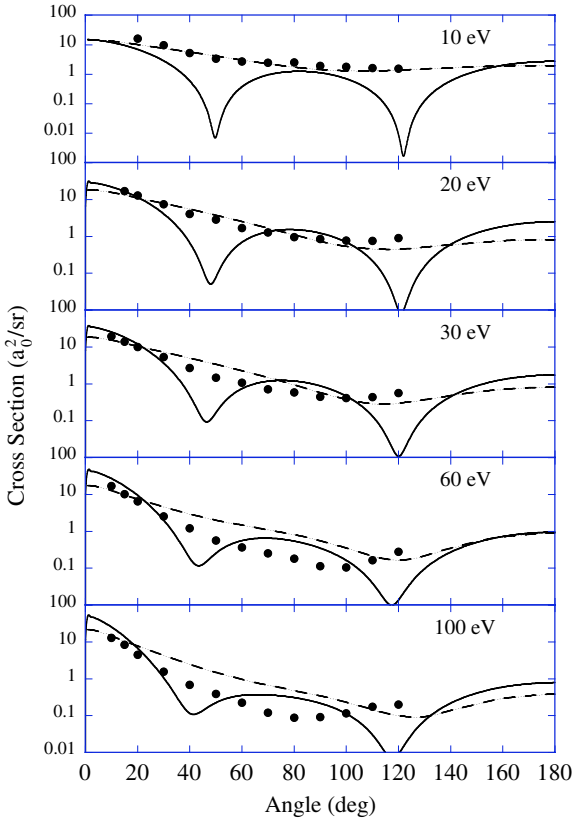

Figure 6. Same as figure 5. Here the theoretical curves are solid $U_S+U_P+U_E$; chain, $U_S+U_P^a+U_E$.

calculated using distorted waves obtained using only the initial and final state static potentials which we label 3DW. The solid curves were obtained from distorted waves calculated including the Perdew–Zunger correlation-polarization potential and the Furness–McCarthy exchange-distortion potential which we label 3DW-CPE and the dotted curves were obtained from distorted waves calculated including the adjustable polarization potential and Furness–McCarthy exchange distortion which we label 3DW-APE. For the adjustable polarization potential, the cutoff parameter for a given electron energy was chosen using figure 7. Of course, this is technically not correct for the two final state electrons since their distorted waves are wavefunctions for elastic scattering from a water ion. However, this was the best we could do since, to our knowledge, there are no experimental results available for differential elastic scattering of an electron from a water ion that could be used to determine the appropriate adjustable parameters for an ion.

For all three measured energies, the theoretical calculations predict a double peak structure for small scattering angles which is also seen in the data. For the lowest energy, all three theoretical predictions are very similar for the first peak near 30° and in good agreement with experiment. For the second peak, the theoretical results are shifted to larger scattering angles as compared to experiment. It is also interesting to note that the ratios of the peak heights are in accord with experiment for the 3DW calculation at the lowest energy but not the two 'improved' theories. All three theoretical calculations predict low-energy large angle structure which is

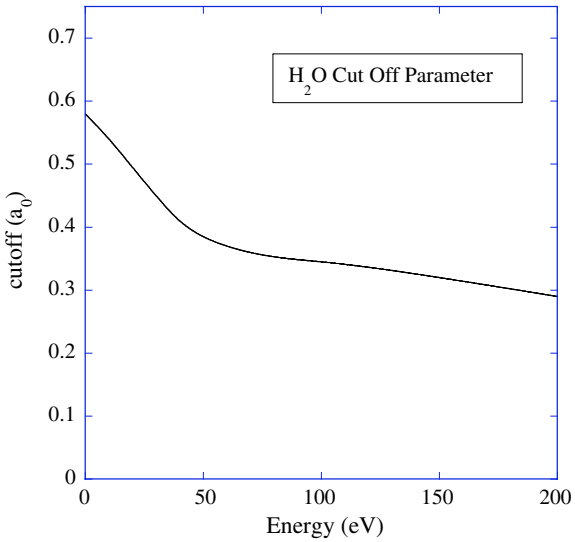

Figure 7. Adjustable cutoff parameter used to calculate differential cross sections shown in figure 6 as a function of the incident electron energy.

not seen in the data. Although none of the calculations are in agreement with experiment for low energy and large scattering angles, overall the 3DW+APE is closest in magnitude which would be expected from the elastic scattering results of figure 6. For the two higher incident-electron energies there is very little difference between the three theoretical calculations. For the higher energies, theory does a better job of predicting the location of the second peak than the first in contrast to the 32.6 eV results. The agreement between experiment and theory for the peak height ratios improves with increasing energy and is quite good for 72.6 eV. For larger scattering angles and higher energy, theory is significantly smaller than experiment. Although the theoretical results do not reproduce all the details of experiment, there is an overall qualitative agreement which is very encouraging for such a complex target.

The fact that polarization and ED (to be referred to as PED) have little effect for the two higher energies is interesting. From figure 5 we saw that PED is important for elastic scattering even at 100 eV. For an ionizing electron with 52.6 eV and symmetric final state energies, we have electron energies of 52.6 eV and 20 eV. For an ionizing electron with 72.6 eV with symmetric final state energies, we have electron energies of 72.6 eV and 30 eV. The fact that PED do not affect the ionization cross sections for these energies indicates that PED are not important in ionizing collisions for electron energies of 20 eV and higher while they have a significant effect on the shape of the 20 eV elastic scattering cross sections. Clearly elastic scattering is more sensitive to PED than ionization.

Figure 9 compares experimental and theoretical results for the asymmetric geometry. Traditionally a small angle peak for asymmetric scattering is called the binary peak and a large angle peak is called the recoil peak. As discussed in the experimental section, the experimental results show a single binary peak and a recoil peak for the lowest energy and a double binary peak for the two higher energies. The theoretical calculations predict a double binary peak for all energies plus some additional structure which develops as the energy increases. Interestingly, the theory predicts a recoil peak for the highest and lowest energy but not for 67.6 eV in contrast to experiment which has the largest recoil peak at 67.6 eV. Contrary

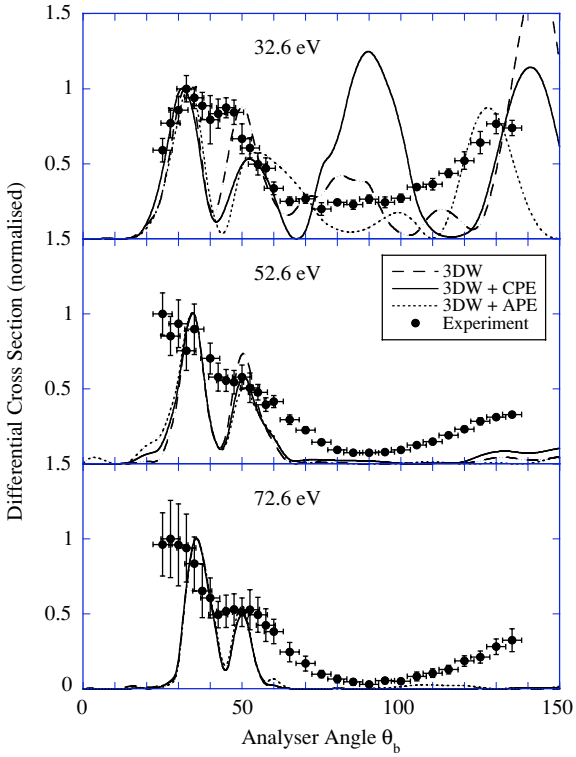

Figure 8. Comparison of experimental and theoretical results for a coplanar symmetric geometry. For details, see text.

to expectations, experiment and theory are in best accord for the lowest energy. This is most likely related to the results for elastic scattering cross sections for which the best agreement was for the lowest energy and agreement got worse with increasing energy which suggests that the distorted waves used in the calculation are more accurate for low energies than for high energies. Except for the double binary peak, the 3DW-APE is in very good agreement with experiment for 27.6 eV which is consistent with the elastic scattering results of figure 6. The 3DW-CPE is in better accord with the binary peak for 27.6 eV in that the first binary peak is more like a 'shoulder', and it is the best for predicting the binary peak height ratios for the two higher energies even though the peak locations are incorrect. Again the encouraging aspect is that there is an overall qualitative agreement between experiment and theory.

An odd feature of the theoretical results lies in the fact that PED plays the biggest role for the highest energy in asymmetric collisions whereas they play no role at the highest energy for symmetric scattering. The reason for this can be directly attributed to the final state 5 eV ejected electron. Recall that for symmetric scattering, we found that PED had no effect for electrons with energies 20 eV and higher. For figure 9, the electron energies in eV are (27.2, 10, 5), (67.6, 50, 5) and (107.6, 90, 5). For the two highest energies, we would expect that only the 5 eV electron should be affected by PED. We verified that this was indeed the case by performing calculations with PED turned on for all three electrons and then for only the 5 eV electron. The results of these two calculations were almost the same for the two higher energies. It is however not clear why PED for the 5 eV electron would have

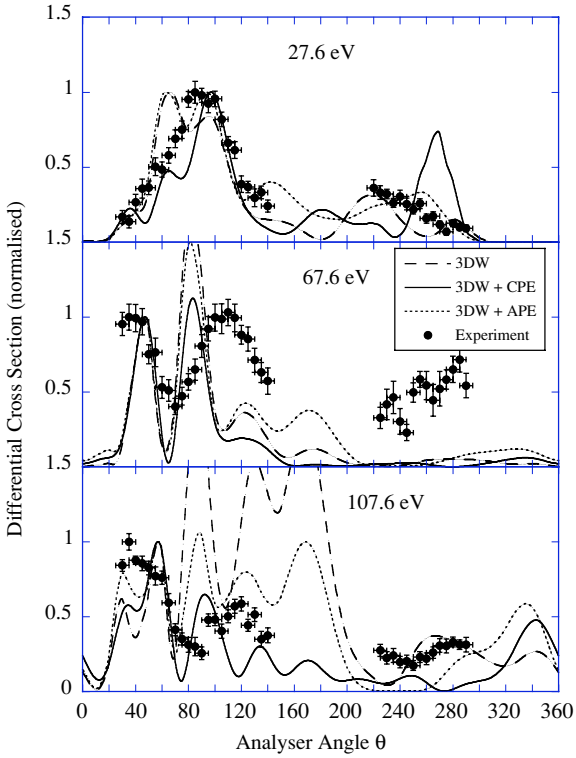

Figure 9. Comparison of experimental and theoretical results for the coplanar asymmetric geometry. For details, see text.

a larger impact at 107.6 eV than for lower incident-electron energies. On the other hand, all the structure seen in the 107.6 eV theoretical results clearly indicates strong interference effects in the scattering amplitudes which logically could be more sensitive to small changes in the wavefunctions. The really good thing, however, is that the large effect of PED on the 5 eV electron significantly improved agreement between experiment and theory at 107.6 eV particularly for the 3DW-CPE calculation which is, at least, in qualitative agreement with experiment whereas the agreement is really terrible otherwise. These results suggest that the lack of agreement between experiment and theory for 107.6 eV probably stems not from the 5 eV distorted wave, but rather from the higher energy distorted waves.

5. Summary and conclusions

The conclusions that can be drawn from these studies indicate that the 3DW model for this polyatomic target has included significant contributions to the physics of the interactions, but that there are deficiencies which need to be addressed. By comparing with elastic scattering cross sections, it was found that the method used to calculate distorted waves is more accurate for low energies than high which is exactly the opposite of our experience for atomic ionization. This has the interesting effect of producing better agreement between experiment and theory for electron impact ionization of polyatomic molecules at low incident-electron energies than high. While there are clear discrepancies between measured data and theory in the results

presented here, overall there is a qualitative agreement between theory and experiment which we find encouraging. H_2O is a polyatomic molecule and so it is very challenging to calculate the ionization cross sections accurately, whereas the experiments are also difficult due to the effects of the molecules on the electron beam over time. The results presented here clearly show that such difficulties can be overcome, and open up the possibility of new experiments and theory being possible for even more complex molecular targets in the near future.

Acknowledgments

CK, MH and AM would like to thank the University of Manchester and the EPSRC for providing funding for the experimental work at Manchester. DS, JG and DM would also like to thank the US National Science Foundation grant for providing funding for the theoretical work which is carried out in Rolla under grant PHY-0456528.

References

[1] McCarthy I E and Weigold E 1976 *Phys. Rep.* **27** 275
[2] Lahmam-Bennani A 1991 *J. Phys. B: At. Mol. Opt. Phys.* **24** 2401
[3] Coplan M A, Moore J H and Doering J P 1994 *Rev. Mod. Phys.* **66** 985
[4] Ullrich J, Moshammer R, Dorn A, Dörner R, Schmidt L Ph H and Schmidt-Böcking H 2003 *Rep. Prog. Phys.* **66** 1463
[5] Jagutzki O, Spielberger L, Dörner R, Nüttgens S, Mergel V, Schmidt-Böcking H, Ullrich J, Olson R E and Buck U 1996 *Z. Phys. D* **36** 5
[6] Gao J, Madison D H and Peacher J L 2005 *Phys. Rev.* A **72** 020701(R)
[7] Gao J, Peacher J L and Madison D H 2005 *J. Chem. Phys.* **123** 204302
[8] Champion C, Hanssen J and Hervieux P A 2001 *Phys. Rev.* A **63** 052720
[9] Champion C, Hanssen J and Hervieux P A 2005 *Phys. Rev.* A **72** 059906
[10] Weigold E, Hood S T and Teubner P J O 1973 *Phys. Rev. Lett.* **30** 475
[11] Weigold E, Hood S T, McCarthy I E and Teubner P J O 1973 *Phys. Lett.* **44A** 531
[12] Murray A J 2005 *J. Phys. B: At. Mol. Opt. Phys.* **38** 1999
[13] Chérid M, Lahmam-Bennani A, Duguet A, Zurales R W, Lucchese R R, Dal Cappello M C and Dal Cappello C 1989 *J. Phys. B: At. Mol. Opt. Phys.* **22** 3483
[14] Jung K, Schubert E, Paul D A L and Ehrhardt H 1975 *J. Phys. B: At. Mol. Phys.* **8** 1330
[15] Hussey M J and Murray A J 2002 *J. Phys. B: At. Mol. Opt. Phys.* **35** 3399
[16] Avaldi L, Camilloni R, Fainelli E and Stefani G 1992 *J. Phys. B: At. Mol. Opt. Phys.* **25** 3551
[17] Doering J P and Yang J 1996 *Phys. Rev.* A **54** 3977
[18] Rioual S, Nguyen Vien G and Pochat A 1996 *Phys. Rev.* A **54** 4968
[19] Hussey M J and Murray A J 2005 *J. Phys. B: At. Mol. Opt. Phys.* **38** 2965
[20] Milne-Brownlie D S, Cavanagh S J, Lohmann B, Champion C, Hervieux P A and Hanssen J 2004 *Phys. Rev.* A **69** 032701
[21] Murray A J, H Turton B C and Read F H 1992 *Rev. Sci. Instrum.* **63** 3346
[22] Murray A J and Read F H 1993 *Phys. Rev.* A **47** 3724
[23] Murray A J and Cvejanovic D 2003 *J. Phys. B: At. Mol. Opt. Phys.* **36** 4875
[24] Murray A J 2005 *Phys. Rev.* A **72** 062711
[25] Newport 325 temperature controller, Newport Corp. 1791 Deere Avenue, Irvine, CA 92606, USA
[26] Gao J, Madison D H and Peacher J L 2005 *J. Chem. Phys.* **123** 204314
[27] Gao J, Madison D H and Peacher J L 2006 *J. Phys. B: At. Mol. Opt. Phys.* **39** 1275
[28] Schmidt M W *et al* 1993 *J. Comput. Chem.* **14** 1347
[29] Furness J B and McCarthy I E 1973 *J. Phys. B: At. Mol. Opt. Phys.* **6** 2280
[30] Perdew J P and Zunger A 1981 *Phys. Rev.* B **23** 5048
[31] Padial N T and Norcross D W 1984 *Phys. Rev.* A **29** 1742
[32] Danjo A and Nishimura H 1985 *J. Phys. Soc. Japan* **54** 1224